The Canadian Mineralogist
Vol. 42, pp. 1871-1880 (2004)

THE PYROPHANITE–ECANDREWSITE SOLID-SOLUTION: CRYSTAL STRUCTURES OF THE $Mn_{1-x}Zn_xTiO_3$ SERIES ($0.1 \leq x \leq 0.8$)

ROGER H. MITCHELL[§] AND RUSLAN P. LIFEROVICH[¶]

Department of Geology, Lakehead University, 955 Oliver Road, Thunder Bay, Ontario P7B 5E1, Canada

ABSTRACT

The crystal structure of members of the pyrophanite–ecandrewsite solid-solution series, $Mn_{1-x}Zn_xTiO_3$ ($0.1 \leq x \leq 0.8$ *apfu*), synthesized by ceramic methods in air at ambient pressure, has been characterized by Rietveld analysis of powder X-ray-diffraction patterns. All of these compounds crystallize with the ilmenite structure and adopt space group $R\bar{3}$. The maximum solubility of Zn in $MnTiO_3$ is considered to be ~0.8 *apfu* Zn, as compounds with greater Zn content do not form. Data are given for cell dimensions and atom coordinates, together with bond lengths, volumes and distortion indices for all coordination polyhedra. Within the solid-solution series, unit-cell parameters and volumes decrease linearly from those of $MnTiO_3$ with increasing $ZnTiO_3$ content. All compounds consist of distorted AO_6 and TiO_6 polyhedra, and, in common with pyrophanite and ilmenite, the former are the more distorted. Displacement of (Mn,Zn) and Ti from the centers of their coordination polyhedra increases with increasing Zn content. The interlayer distance across the vacant octahedral site in the TiO_6 layer decreases with entry of the smaller Zn cation into the AO_6 octahedra. The synthetic titanates are analogues of iron-free manganoan ecandrewsite and zincian pyrophanite occurring in peralkaline syenites at Pilansberg, in South Africa, and Poços de Caldas, in Brazil.

Keywords: ecandrewsite, pyrophanite, titanate, order, ilmenite group, distorted octahedra, crystal structure, Rietveld refinement.

SOMMAIRE

Nous avons determiné la structure cristalline de membres de la solution solide pyrophanite–ecandrewsite, $Mn_{1-x}Zn_xTiO_3$ ($0.1 \leq x \leq 0.8$ *apfu*), synthétisée selon des méthodes céramiques dans l'air à pression ambiante, par affinement de Rietveld de données obtenues par diffraction X sur poudres. Tous ces composés cristallisent avec la structure de l'ilmenite et adoptent donc le groupe spatial $R\bar{3}$. La solubilité maximum de Zn dans le $MnTiO_3$ serait environ 0.8 *apfu* Zn, parce que des composés ayant une teneur plus élevée de Zn ne se sont pas formés. Nous fournissons les données requises pour décrire les paramètres réticulaires, les coordonnées des atomes, les longueurs des liaisons, et les volumes et les indices de distorsion de tous les polyèdres de coordinence. Dans la solution solide, les paramètres réticulaires et les volumes de la maille élémentaire diminuent de façon linéaire à partir de ceux de $MnTiO_3$ à mesure que la proportion de $ZnTiO_3$ augmente. Tous ces composés contiennent des polyèdres de coordinence AO_6 et TiO_6 difformes; tout comme pour la pyrophanite et l'ilménite, le polyèdre AO_6 est le plus difforme des deux. Le déplacement de (Mn,Zn) et de Ti des centres des polyèdres de coordinence augmente avec l'augmentation de la proportion du Zn. La distance intercouche traversant la lacune dans le site octaédrique de la couche d'octaèdres TiO_6 diminue à mesure que le Zn entre dans le site A des octaèdres AO_6. Les titanates synthétiques sont les analogues de l'ecandrewsite manganifère dépourvue de fer et de la pyrophanite zincifère que nous retrouvons dans les syénites hyperalcalines à Pilansberg, en Afrique du Sud, et à Poços de Caldas, au Brésil.

(Traduit par la Rédaction)

Mots-clés: ecandrewsite, pyrophanite, titanate, ordre, groupe de l'ilménite, octaèdre difforme, structure cristalline, affinement de Rietveld.

§ *E-mail address*: rmitchel@lakeheadu.ca
¶ *Permanent address*: Geological Institute, Kola Science Centre, Russian Academy of Sciences, 14 Fersmana Street, RU–184200 Apatity, Russia.

Introduction

Mitchell & Liferovich (2004) have recently reported the first occurrence in igneous rocks of minerals belonging to the ecandrewsite ($ZnTiO_3$) – pyrophanite ($MnTiO_3$) solid-solution series. It was assumed that these minerals belong to the ilmenite group and adopt the space group $R\bar{3}$. Unfortunately, most of the crystals are complexly zoned on a micrometer scale, and it was not possible to obtain material suitable for determination of their crystal structures. Surprisingly, crystal-structure data for this solid-solution series are not available. Accordingly, we have synthesized analogues of the natural materials to determine their crystal structure and the crystallochemical effects of the replacement of Mn^{2+} by the smaller Zn^{2+} cation. This work is the first investigation of the synthetic $Mn_{1-x}Zn_xTiO_3$ solid solution.

Background Information

Natural titanates of Zn and Mn

The compositions of naturally occurring representatives of minerals in the system $FeTiO_3$–$MnTiO_3$–$ZnTiO_3$ are plotted in Figure 1. The natural samples form near-complete $(Mn_{1-x}Zn_x)TiO_3$ and $(Fe_{1-x}Zn_x)TiO_3$, and continuous $(Fe_{1-x}Mn_x)TiO_3$ solid-solution series.

Individual crystals and complex aggregates representative of the extensive ecandrewsite – pyrophanite

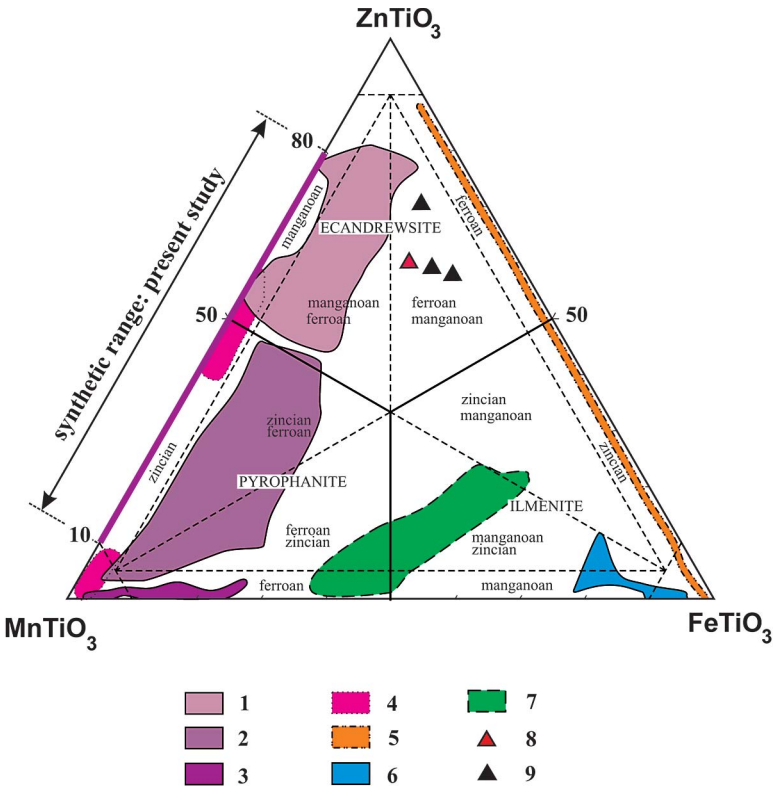

FIG. 1. Composition of ecandrewsite and related ilmenite-group minerals in terms of the proportions of Zn–Mn–Fe (mol.%). Samples 1–3: consecutive generations from lujavrite, Pilansberg sodic peralkaline complex, South Africa, from early ecandrewsite to late pyrophanite (Mitchell & Liferovich 2004); 4 Poços de Caldas lujavrite, Brazil (*in prep.*); 5 kyanite schist, Death Valley, California (Whitney *et al.* 1993); 6 syenite and material from miarolitic cavities in peralkaline rhyolite, Cape Ashizuri, Japan (Nakashima & Imaoka 1998); 7 material from miarolitic cavities in the Kuiqi alkaline granite, Fujian, China (Suwa *et al.* 1987); 8 type-locality ecandrewsite from siliceous metasedimentary units, Melbourne Rockwell mine, Little Broken Hill (Birch *et al.* 1988); 9 San Valentin mine (Birch *et al.* 1988).

(± ilmenite) solid-solution series have been recognized recently in highly evolved nepheline syenite (lujavrite) from the Pilansberg peralkaline complex, in South Africa, and similar trachytoid sodic peralkaline syenite from the Poços de Caldas complex, in Brazil (Mitchell & Liferovich 2004).

Ecandrewsite–ilmenite solid solutions typically occur in metamorphic rocks of a low to middle grade of metamorphism (Whitney *et al.* 1993), although zincian manganoan ilmenite and ferroan zincian pyrophanite are found lining miarolitic cavities in peralkaline granite and rhyolite (Suwa *et al.* 1987, Nakashima & Imaoka 1998). Ternary compositions with near-equal amounts of Mn, Fe, and Zn are not known to exist in nature. In addition, only very limited $^{[vi]}$Mg-for-$^{[vi]}$Zn diadochy is observed in the natural examples (Mitchell & Liferovich 2004). Given that $^{[vi]}R_{Mg} \approx {}^{[vi]}R_{Zn} < {}^{[vi]}R_{Fe} < {}^{[vi]}R_{Mn}$ [0.72, 0.74, 0.78, and 0.83 Å for divalent cations, respectively (Shannon 1976)], this compositional gap seems to result from the different geochemical behavior of Mg, Fe^{2+}, Mn^{2+} and Zn, rather than for crystallochemical reasons.

Ternary titanates: structural outline

The ilmenite structure is an ordered derivative of the *aristotype* corundum structure (Barth & Posnjak 1934). Typically, the ilmenite structure is adopted by $A^{2+}B^{4+}O_3$ compounds, where $^{[vi]}R_A$ is close to $^{[vi]}R_B$ and $^{[vi]}R_A$ is much smaller than the radius of the oxygen anion, resulting in a Goldshmidt tolerance factor higher than 0.75 (Mitchell 2002). The ilmenite structure is based on layers of hexagonally close-packed atoms of oxygen with cations occupying two thirds of the available octahedral interstices. In contrast to the fully disordered corundum structure (space group $R\bar{3}c$), the ilmenite structure results from equal amounts of divalent and tetravalent cations, which are ordered at the octahedral sites, and alternate along the *c* dimension of the unit cell. A pair of AO_6 (A = Fe^{2+}, Mg, Mn, Zn, Co, or Ni) and TiO_6 octahedra share a (001) face, and each octahedron in the ilmenite structure shares an edge with the same type of octahedron and three edges with the other octahedra (Fig. 2a). The stacking sequence of cations along $[001]_h$ of this structure is *A*–Ti–□–Ti–*A*–□, and Ti–Ti–□ or *A*–*A*–□ parallel to (111), resulting in a $R\bar{3}$ rhombohedral cell.

In common with corundum, cations in the $R\bar{3}$ structure are displaced from the centers of both octahedra, resulting in distortion of the coordination polyhedra. Various styles of distortion are known for ilmenite-structure compounds. The AO_6 polyhedron may be more distorted than the BO_6 polyhedron or *vice versa*, *e.g.*, in ilmenite *sensu stricto*, distortion of the FeO_6 octahedron is significantly lower than that of the TiO_6 octahedron (Mitchell 2002). As both cation sites lie on threefold axes, each one has a single variable atomic positional parameter, *z*. Deviations of *z* from $^1/_3$ and $^1/_6$ for the *A* and Ti atoms, respectively, are indicative of "puckering" of cation layers above and below planes parallel to (001) (Wechsler & Prewitt 1984).

Further distortion of the corundum structure in $A^{2+}B^{4+}O_3$ compounds can be driven by an increase in intensive parameters (*P*, *T*). The distortion can result in a phase transition to a structure with the *A*–*B*–□–*A*–*B*–□ stacking sequence, both along and orthogonal to $[001]_h$, with the A^{2+} and B^{4+} cations occupying alternating layers. The structure has a *R*3*c* rhombohedral cell and is referred to as the lithium niobate ($LiNbO_3$) structure. This *hettotype* (Mitchell 2002) differs in the mode of connection of octahedra from that occurring in the ilmenite structure (Fig. 2b).

With increasing pressure, ilmenite and lithium niobate ABO_3 compounds can undergo a phase transition to a *Pbnm*-structured perovskite isostructural with $GdFeO_3$ (Linton *et al.* 1999). Phase transformations between the ilmenite, lithium niobate and perovskite structures are complex, and their study is hindered by kinetic factors and hysteresis effects (Mitchell 2002).

Pyrophanite is isostructural with ilmenite at ambient pressure, but at high pressure, it undergoes a phase transition to the lithium niobate structure (Syono *et al.* 1969, Ko & Prewitt 1988). The only crystal-structure study of natural ecandrewsite is that of the holotype, with the composition of $Zn_{0.59}Fe_{0.24}Mn_{0.17}TiO_3$ (Gatehouse & Nesbit 1978). This mineral was found to be isostructural with $R\bar{3}$ ilmenite (Birch *et al.* 1988). The space group of synthetic $ZnTiO_3$ is given as $R\bar{3}$ by Bartram & Slepetys (1961) and as *R*3*c* at unspecified conditions in the JCPDS Powder Diffraction File database (Card No. 26–1500). The former is very poorly defined (R_{Bragg} = 13.5%), and the latter is unlikely to be correct at ambient conditions. Our experimental study shows that $ZnTiO_3$ cannot be formed in air at ambient pressure over the temperature range 700–1300°C. Consequently, we were unable to determine the unit-cell dimensions and space group actually adopted by the $ZnTiO_3$ end-member. Because of the poor quality of data given by Bartram & Slepetys (1961), we consider that the crystal structure of $ZnTiO_3$ is not well established and is thus not considered further in the discussion below.

Experimental and Analytical Methods

Zinc–manganese titanates were synthesized from stoichiometric amounts of high-purity $MnCO_3$, ZnO, Fe_2O_3, and TiO_2 (all Aldrich Chemical Co.) by solid-state ceramic techniques. The reagents, dried at 120°C (with exception of $MnCO_3$, which was kept at 95°C to avoid decomposition) for several days, were mixed, ground in an agate mortar under acetone, and calcined in air for 12 h at 800°C. Graphite was used to maintain Mn in the reduced (divalent) state. After regrinding, the samples were pelletized at a pressure 10 tonnes per square centimeter, and then sintered in air for 24 h at 900°C.

The compositions of all titanates formed were assessed using a JEOL JSM–5900 scanning electron microscope (SEM) by back-scattered electron imagery (BSE) and quantitative energy-dispersion analysis (EDS). Step-scanned powder X-ray-diffraction (XRD) patterns of the products were obtained at room temperature using a Philips 3710 diffractometer (T = 20°C; radiation Cu$K\alpha$; 2θ range 9°–145°, Δ2θ step 0.02°; counting time per step 4 s) with APD powder-diffraction software.

The XRD patterns were inspected using the Bruker AXS software package EVA to identify the phases present and to confirm that $R\bar{3}$-structured compounds had been produced. Data were further analyzed by Rietveld methods using the Bruker AXS software package TOPAS 2.1 operated in the fundamental parameters mode (Kern & Coelho 1998). Depending upon the presence of impurities, the number of TOPAS 2.1 refined variables ranged up to 45 independent parameters. These included: zero corrections, scaling factors, cell dimensions, positional coordinates of atoms, preferred orientation corrections, crystal size, strain effects, and isotropic thermal parameters. The occupancy factors of all sites were set to 1, except for that of the mixed-occupancy octahedral site *A*, which was set in accordance with initial mixture composition as confirmed by SEM–EDS analysis. Attempts to refine the occupancy of the *B* site assuming entry of Mn^{3+}, Mn^{4+}, or Zn did not indicate their presence within the limits of accuracy of the determination by Rietveld methods.

The ATOMS 6.0 software package (Dowty 1999) was used to determine interaxial angles describing the distortion of coordination polyhedra and selected bond-lengths. The IVTON 2.0 program (Balić-Žunić & Vicković 1996) was employed to characterize the coordination spheres of the cations, volumes of coordination polyhedra, and displacements of cations from the centers of coordination polyhedra.

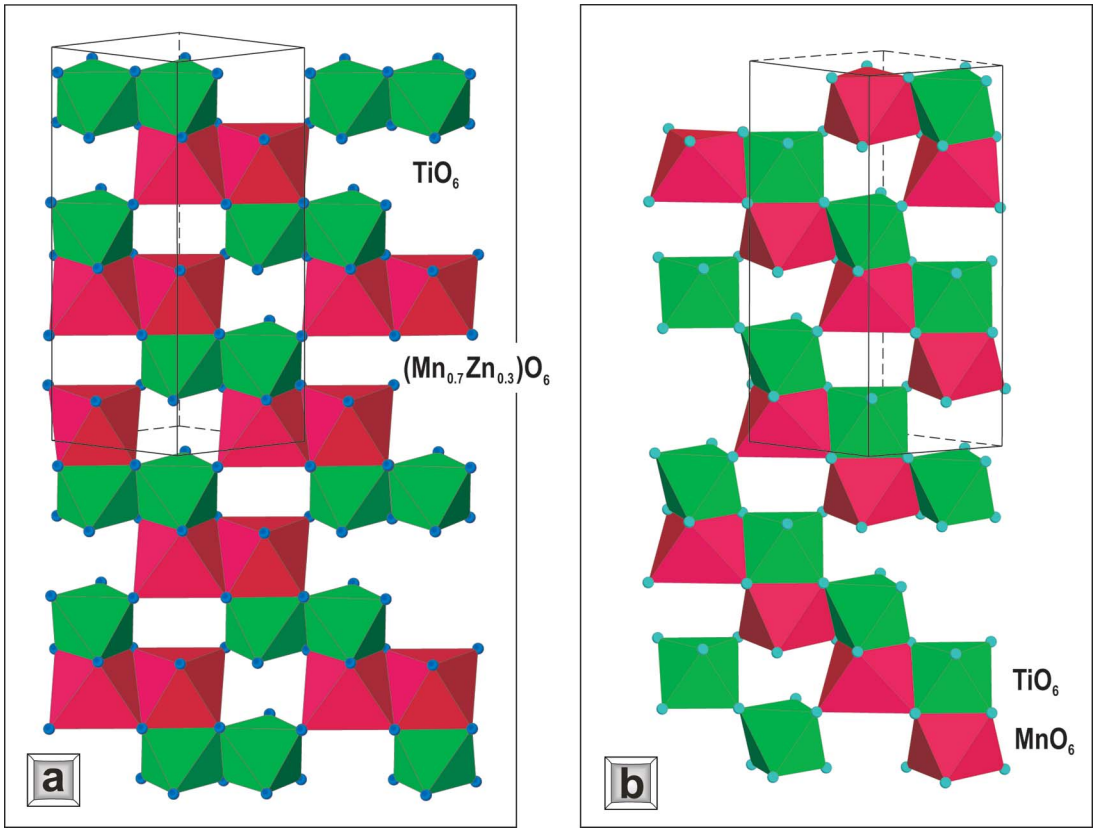

FIG. 2. Projections onto the $(1\bar{1}0)$ plane of portions of the structures of: (a) $R\bar{3}$ synthetic manganoan ecandrewsite ($Mn_{0.3}Zn_{0.7}TiO_3$), obtained in the present study, (b) high-pressure modification of $MnTiO_3$ isostructural with $R3c$ $LiNbO_3$ [data taken from Ko & Prewitt (1988)], illustrating the order and disposition of the face- and corner-sharing octahedra.

RESULTS

Synthetic zinc–manganese titanates

Our study demonstrates that synthesis of the $Mn_{1-x}Zn_xTiO_3$ ($0.1 \le x \le 0.8$) solid-solution series is possible at ambient pressure in air. However, end-member pyrophanite ($MnTiO_3$), ecandrewsite ($ZnTiO_3$), and $Zn_{0.9}Mn_{0.1}TiO_3$ titanate were not formed under our conditions of synthesis in the temperature range 700–1300°C. (N.B.: Commercially available compounds considered by their distributors to be pure $ZnTiO_3$ and $MnTiO_3$ were shown by our X-ray-diffraction methods to be merely mixtures of spinel and oxide matching the ecandrewsite and pyrophanite stoichiometries, respectively: *caveat emptor*).

Synthesis of Fe-bearing titanates also was undertaken, but was unsuccessful under our conditions of synthesis. These compounds might be analogues of naturally occurring zincian manganoan ilmenite, zincian ferroan pyrophanite, and ecandrewsite–ilmenite solid solutions (Fig. 1). We also attempted to synthesize the ternary $Fe_{1/3}Mn_{1/3}Zn_{1/3}TiO_3$ compound. Various combinations of initial components were used, *e.g.*, $FeTiO_3$, $FeCO_3$ + graphite, Fe_2O_3 + graphite, Fe_{metal} + Fe_2O_3, *etc*. None of these Fe-bearing mixtures produced rhombohedral titanates even if we use as a starting material $R\bar{3}$-structured Mn–Zn titanates doped with as little as 0.05 *apfu* Fe. In contrast, quenched synthetic $Zn_{1/2}Mg_{1/2}TiO_3$, $Zn_{1/3}Mg_{1/3}Mn_{1/3}TiO_3$, and $Mg_{1/2}Mn_{1/2}TiO_3$ titanates readily adopt the ordered $R\bar{3}$ ilmenite structure at 1000–1050°C at ambient pressure (*in prep*.).

The powder X-ray-diffraction patterns of all members of the synthetic $Mn_{1-x}Zn_xTiO_3$ ($0.1 \le x \le 0.8$) solid solution (*e.g.*, Fig. 3), contain reflections with (*h*0*l*; *l* odd) resulting from the ordered distribution of A^{2+} and Ti^{4+} in alternate layers of octahedra (Raymond & Wenk 1971). These reflections are forbidden for the fully disordered $R\bar{3}c$ corundum-type structure and the $R3c$ $LiNbO_3$ structure.

For the Rietveld refinement, we used the atom coordinates given by Kidoh *et al.* (1984) for pyrophanite as a starting model. Figure 3 shows the result of a Rietveld refinement of the synthetic titanate $Mn_{0.3}Zn_{0.7}TiO_3$. The crystallochemical characteristics of the synthesized titanates are summarized in Table 1, in conjunction with data for synthetic pure $MnTiO_3$ (Kidoh *et al.* 1984) and $FeTiO_3$ (Wechsler & Prewitt 1984). As expected, our

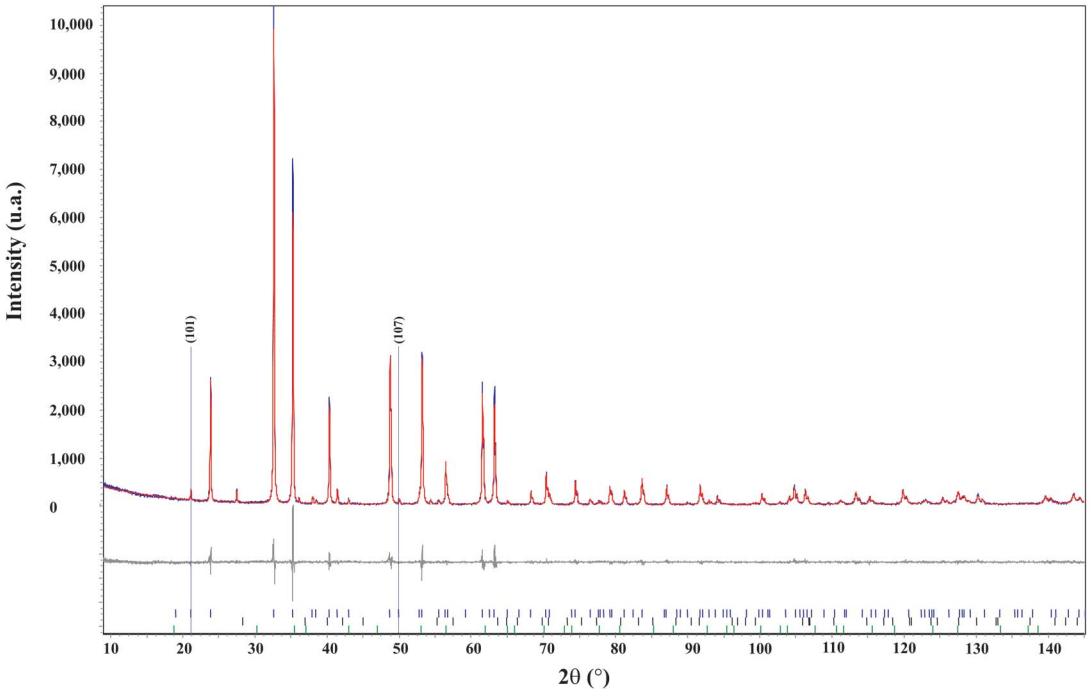

FIG. 3. Rietveld refinement plot (line) of the X-ray powder-diffraction data for $Mn_{0.3}Zn_{0.7}TiO_3$ at room temperature (dots). The vertical bars indicate the Bragg reflections allowed for ordered ilmenite structure (upper row) and the minor phases, rutile and spinel (middle and bottom bars, 1.9 and 2.0 wt.%, respectively). The difference curves between observed and calculated profiles are plotted. For the agreement factors, see Table 1.

TABLE 1. RIETVELD REFINEMENT RESULTS AND UNIT-CELL DIMENSIONS OF SYNTHETIC $(Mn_{1-x}Zn_x)TiO_3$ SOLID-SOLUTION ($0.1 \le x \le 0.8$) AT AMBIENT CONDITIONS

x	Minor phases wt.%	Titanate wt.%	R_{wp}	R_{Bragg}	GOF	DW	a, Å	c, Å	V, Å^3	c/a	t **
0.0 *	-						5.139	14.283	326.7	2.7793	0.786
0.1	Rutile (4.96)	95.04	13.54	2.40	1.38	1.21	5.13058(3)	14.2465(1)	324.765(5)	2.7768	0.783
0.2	Rutile (4.90)	95.10	14.46	2.59	1.37	1.26	5.12512(4)	14.2119(2)	323.290(6)	2.7730	0.780
0.3	Rutile (2.80)	97.20	12.75	2.19	1.39	1.19	5.11892(3)	14.1741(1)	321.649(5)	2.7690	0.777
0.4	Rutile (2.33)	97.67	12.32	2.27	1.37	1.21	5.11293(3)	14.1367(1)	320.051(5)	2.7649	0.774
0.5	Spinel (2.51)	97.49	11.78	1.92	1.34	1.20	5.10630(4)	14.0992(2)	318.375(6)	2.7611	0.771
0.6	Rutile (2.06) Spinel (1.79)	96.15	12.41	2.11	1.35	1.24	5.10040(4)	14.0630(2)	316.824(6)	2.7572	0.767
0.7	Rutile (1.89) Spinel (2.0)	96.11	11.14	2.13	1.36	1.19	5.09472(4)	14.0302(2)	315.381(6)	2.7539	0.764
0.8	Rutile (1.72) Spinel (1.80)	96.48	10.80	2.29	1.40	1.16	5.08849(4)	13.9937(2)	313.790(7)	2.7501	0.761
-											
1.0	Rutile, Spinel ¶	-	-	-	-	-	-	-	-	-	0.755
$FeTiO_3$ ***							5.0884(1)	14.0855(4)	315.84(1)	2.7682	0.769

-: no data available. * Single-crystal data (Kidoh *et al.* 1984). ** Tolerance factor for ABO_3 compounds, $t = (R_O + R_A) / [\sqrt{2}\,(R_O + R_B)]$ (Goldschmidt 1926), where R_A, R_B and R_O are the six-fold ionic radii of A, B and O, respectively; relevant average values of R_A are used for the $(Mn_{1-x}Zn_x)TiO_3$ series. *** Data after Wechsler & Prewitt (1984). ¶ ± an armalcolite-like phase.

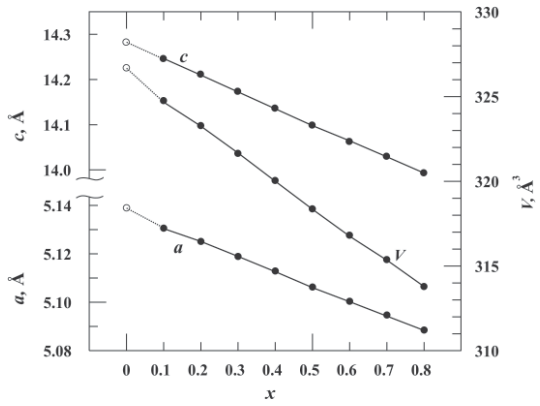

FIG. 4. The $Mn_{1-x}Zn_xTiO_3$ series: variations of the unit-cell parameters and unit-cell volume with composition. Data for $x = 0$ are from Kidoh *et al.* (1984). Note that the error bars are less than the size of dots employed in the plot (Table 1).

study shows that entry of the smaller Zn^{2+} cation at the $A_{(Mn,Zn)}$ site results in a regular decrease of the unit-cell parameters and unit-cell volume with increasing Zn content (Fig. 4).

Atom coordinates and isotropic thermal parameters are summarized in Table 2. Bond lengths within coordination octahedra, polyhedra volumes, displacements (shifts) of $^{[vi]}A^{2+}$ and $^{[vi]}Ti^{4+}$ atoms from the centers of coordination polyhedra and bond-length distortion indices for representative compounds are listed in Table 3, with comparative data for synthetic $MnTiO_3$ (Kidoh *et al.* 1984) and $FeTiO_3$ (Wechsler & Prewitt 1984). Selected bond-lengths and framework angles are given in Appendix 1.

CRYSTAL CHEMISTRY

We employ the distortion index introduced by Shannon (1976) to illustrate bond-length distortion in the polyhedra . The index is defined as $\Delta_n = 1/n \bullet \Sigma\{(r_i - \bar{r}) / \bar{r}\}^2 \bullet 10^3$, where r_i and $\bar{r}$ are individual and average bond-lengths in the polyhedron, respectively. To characterize deviations from the ideal bond-angles in regular octahedra, we calculate the bond-angle variance index, δ_n, where $\delta_n = [\Sigma\,(\theta_i - 90)^2]/(n - 1)$, and θ_i are the bond angles at the central atom of an octahedron (Robinson *et al.* 1971). The indices calculated, plus bond-angles within coordination polyhedra, are given in Table 4.

As expected, the <*A*–O> and <Ti–O> distances (Table 3) decrease with increasing x, resulting in a linear decrease of the unit-cell dimensions and unit-cell volume through the series (Table 1, Fig. 4). Polyhedron volumes change in a similar manner, with the exception of the most Zn-rich titanate, $Mn_{0.2}Zn_{0.8}TiO_3$, which exhibits a slightly low volume for the TiO_6 octahedron and a somewhat high volume for the AO_6 octahedron

(Table 3, Figs. 5a, b). With increasing x, the z_A and z_{Ti} coordinates deviate antipathetically from the values of $^1/_3$ and $^1/_6$, respectively (Table 2). This feature indicates increasing deformation of both AO_6 and TiO_6 coordination polyhedra, which can be referred to as "puckering" of cation layers above and below planes parallel to (001) (Wechsler & Prewitt 1984). The change in z coordinate is in agreement with the calculated shift of the atoms from the centers of the coordination polyhedra (Table 3, Figs. 5a, b). As the $|\,^1/_3 - z_A{}^{2+}\,|$ values are significantly less than those of $|^1/_6 - z_{Ti}{}^{4+}|$, the layer consisting of TiO_6 octahedra is considerably more deformed than the layer composed of AO_6 octahedra. The A–A distance across the vacant octahedral site in the TiO_6 layer decreases with entry of the smaller $^{[vi]}Zn^{2+}$ cation into the A site. The A–Ti distance between nearest metal sites also decreases with x (Appendix 1).

TABLE 2. ATOMIC POSITIONS, ISOTROPIC THERMAL PARAMETERS (B_{iso}) OF SYNTHETIC $(Mn_{1-x}Zn_x)TiO_3$ SOLID-SOLUTION ($0.1 \le x \le 0.8$) AT AMBIENT CONDITIONS

Position	Sample	x	y	z	B_{iso} [Å^2]
$^{[vi]}A$	x = 0 *	0	0	0.36002(1)	
	x = 0.1	0	0	0.36031(8)	0.5(6)
	x = 0.3	0	0	0.36072(8)	0.5(1)
	x = 0.5	0	0	0.36093(7)	0.7(2)
	x = 0.7	0	0	0.36125(7)	1.0(2)
	x = 0.8	0	0	0.36134(7)	0.4(6)
	$FeTiO_3$ **	0	0	0.35537(2)	0.6
$^{[vi]}$Ti	x = 0 *	0	0	0.14758(1)	
	x = 0.1	0	0	0.14820(9)	0.3(3)
	x = 0.3	0	0	0.14805(9)	0.4(3)
	x = 0.5	0	0	0.14779(9)	0.2(3)
	x = 0.7	0	0	0.14723(8)	0.5(3)
	x = 0.8	0	0	0.14687(8)	0.6(3)
	$FeTiO_3$ **	0	0	0.14640(2)	0.5
O1	x = 0 *	0.3189(1)	0.0310(1)	0.24393(3)	
	x = 0.1	0.3205(5)	0.0313(7)	0.2437(4)	0.4(6)
	x = 0.3	0.3206(5)	0.0302(6)	0.2435(4)	0.5(5)
	x = 0.5	0.3204(5)	0.0297(6)	0.2442(3)	0.2(5)
	x = 0.7	0.31994(5)	0.0280(6)	0.2438(3)	0.5(5)
	x = 0.8	0.31952(5)	0.0274(7)	0.2430(5)	0.5(2)
	$FeTiO_3$ **	0.3174(2)	0.0233(2)	0.24506(5)	0.6

$A = {}^{[vi]}(Mn_{1-x}Zn_x)$. * Data from the single-crystal refinement of Kidoh *et al.* (1984). ** Data from the single-crystal refinement of Wechsler & Prewitt (1984).

The $Mn_{1-x}Zn_xTiO_3$ series consist of coordination polyhedra that are distorted in a manner similar to those occurring in pyrophanite and ilmenite. The AO_6 octahedra exhibit a lesser degree of distortion than the TiO_6 octahedra, as illustrated by indices of bond-length distortion (Table 3, Fig. 5). Overall distortion of the AO_6 and TiO_6 octahedra depends on the extent of Zn-for-Mn substitution and increases with increasing Zn. Indices of bond-angle variance are less sensitive to entry of $^{[vi]}Zn^{2+}$ at the A site and vary irregularly (Table 4).

Whereas the unit-cell parameters and volumes of the compounds in the pyrophanite–ecandrewsite solid solution evolve linearly (Fig. 4), the overall trends of crystallochemical characteristics are complicated by the anomalies observed for the Zn-rich titanate ($Mn_{0.2}Zn_{0.8}TiO_3$). As further increases in Zn content result in a collapse of the ilmenite structure to a mixture of spinel and rutile (± an armalcolite-like titanate), we assume the $Mn_{0.2}Zn_{0.8}TiO_3$ compound to be metastable. Note that natural iron-free manganoan ecandrewsite from the Pilansberg complex (Mitchell & Liferovich 2004) contains a maximum of 0.78 *apfu* Zn (Fig. 1). Further entry

TABLE 3. POLYHEDRON BOND-LENGTHS AND VOLUMES OF SYNTHETIC $(Mn_{1-x}Zn_x)TiO_3$ SOLID-SOLUTION ($0.1 \le x \le 0.8$) AT AMBIENT CONDITIONS

		x = 0*	x = 0.1	x = 0.3	x = 0.5	x = 0.7	x = 0.8	$FeTiO_3$
AO_6 octahedron								
3 × A–O1	Å	2.110(1)	2.104(4)	2.091(3)	2.078(3)	2.066(3)	2.065(3)	2.0778(8)
3 × A–O1	Å	2.280(1)	2.286(5)	2.285(4)	2.272(4)	2.272(4)	2.276(5)	2.2013(8)
<A–O1>	Å	2.195(1)	2.195(5)	2.188(4)	2.175(4)	2.169(3)	2.170(4)	2.1396(8)
V_{AO6}	Å^3	13.350(1)	13.344(5)	13.217(6)	12.972(5)	12.864(5)	12.892(6)	12.562(1)
Shift in A		0.381	0.384	0.388	0.389	0.392	0.396	0.310
Δ_{AO6}		1.500	1.719	1.965	1.989	2.255	2.363	0.833
TiO_6 octahedron								
3 × Ti–O1	Å	1.877(1)	1.871(4)	1.865(4)	1.863(4)	1.857(4)	1.849(4)	1.8744(8)
3 × Ti–O1	Å	2.084(1)	2.078(5)	2.073(4)	2.073(4)	2.069(4)	2.060(5)	2.0886(8)
<Ti–O1>	Å	1.980(1)	1.974(5)	1.969(4)	1.968(4)	1.963(4)	1.955(5)	1.9815(8)
V_{TiO6}	Å^3	9.972(1)	9.898(5)	9.820(5)	9.815(4)	9.718(4)	9.583(5)	10.001(1)
Shift in Ti		0.273	0.263	0.264	0.266	0.273	0.274	0.285
Δ_{TiO6}		2.731	2.748	2.790	2.847	2.916	2.914	2.921

$A = {}^{[vi]}(Mn_{1-x}Zn_x)$. Shifts in A and Ti are the distances to the central atoms. Δ_n: Polyhedron bond-length distortion, $\Delta_n = 1/n \cdot \Sigma\{(r_i - \bar{r}) / \bar{r}\}^2 \cdot 10^3$, where r_i and $\bar{r}$ are individual and average bond-lengths, respectively (Shannon 1976). * Data after Kidoh *et al.* (1984). Data for $FeTiO_3$ are after Wechsler & Prewitt (1984).

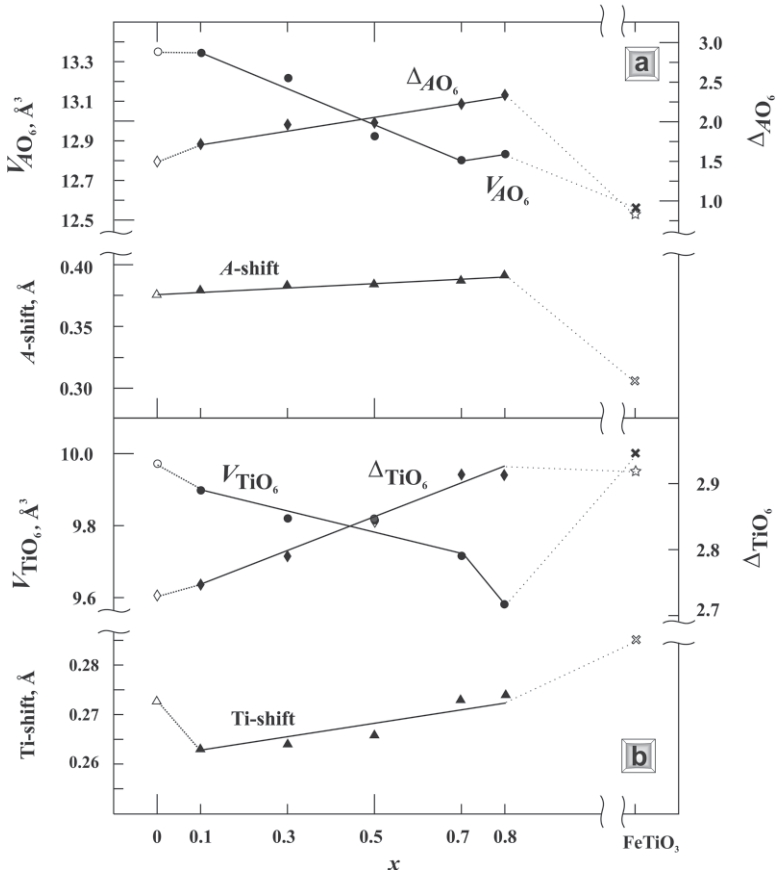

FIG. 5. The $Mn_{1-x}Zn_xTiO_3$ series: variation in the volume of coordination polyhedra, their distortion parameters (see text), and displacements of the *A* and Ti cations from the centers of the coordination polyhedra with composition. Data for pyrophanite and ilmenite are adopted from Kidoh *et al.* (1984) and Wechsler & Prewitt (1984), respectively.

of Zn^{2+} (up to 0.81 *apfu* Zn) into the *A* site of natural ecandrewsite seems to be possible only in conjunction with Fe^{2+} (Fig. 1). In this case, the capacity of the structure of manganoan ecandrewsite for Zn is increased by the dimensional effect of the coentry of the larger Fe^{2+} ion [$^{[vi]}R = 0.78$ Å (Shannon 1976)] at the *A* site, resulting in an increase in the average ionic radius of the $^{[vi]}A^{2+}$ cations. Consequently, this coentry decreases the Goldschmidt tolerance factor in the most zincian natural Fe–Mn–Zn titanate known, to the range tolerable for the ilmenite structure. This observation is supported by the larger, but still limited, capacity for Zn in Mn-poor ilmenite–ecandrewsite solid-solutions occurring in pelitic schists (Whitney *et al.* 1993). Ecandrewsite from Death Valley, California, contains up to 0.85 *apfu* Zn (Fig. 1). The most zincian composition described from that locality has a total of 1.04 *apfu* (Fe + Zn), implying that some Fe must be oxidized and enters the $^{[vi]}Ti^{4+}$ sites, thus demonstrating incipient instability of the structure, and suggesting that this compound is metastable in a similar manner to $Zn_{0.8}Mn_{0.2}TiO_3$.

CONCLUSIONS

The experimentally obtained limit of substitution of Zn for Mn in the structure of Fe-free pyrophanite is *ca.* 0.8 *apfu* Zn at ambient pressure. This limit is in good agreement with the composition of natural iron-poor to iron-free manganoan ecandrewsite occurring in the subvolcanic Pilansberg lujavrites (highly evolved hypersolvus trachytic nepheline syenites), South Africa (Fig. 1, Mitchell & Liferovich 2004). The empirical range of the Goldschmidt tolerance factors for ABO_3 titanates of the first-row transition metals adopting or-

TABLE 4. SELECTED BOND-ANGLES OF SYNTHETIC $(Mn_{1-x}Zn_x)TiO_3$ SOLID-SOLUTION ($0.1 \le x \le 0.8$) AT AMBIENT CONDITIONS

x =		0*	0.1	0.3	0.5	0.7	0.8	$FeTiO_3$
AO_6 octahedron								
3 × O–*A*–O	°	72.95	73.00	73.00	73.20	73.18	72.88	75.67
3 × O–*A*–O	°	91.95	91.70	91.54	91.09	90.99	91.20	90.93
3 × O–*A*–O	°	88.22	88.07	88.10	87.75	88.03	88.44	89.16
3 × O–*A*–O	°	103.28	103.28	103.38	103.79	103.73	103.44	101.39
δ_{AO6}		129.28	128.72	129.27	130.54	129.90	130.25	91.81
TiO_6 octahedron								
3 × O–Ti–O	°	81.14	81.77	81.97	81.69	81.76	81.99	80.56
3 × O–Ti–O	°	80.92	80.85	80.78	81.04	80.84	80.39	82.07
3 × O–Ti–O	°	94.81	94.64	94.16	94.23	93.56	93.01	93.28
3 × O–Ti–O	°	101.88	101.63	101.89	101.81	102.41	103.03	102.35
δ_{TiO6}		88.70	84.07	84.05	83.65	86.86	91.46	85.99

$A = {}^{[VI]}(Mn_{1-x}Zn_x)$. δ_a, the bond-angle variance (Robinson *et al.* 1971) is defined as $\delta = \Sigma[(\theta_i - 90)^2/(n-1)]$, where θ_i are bond angles. * Data after Kidoh *et al.* (1984). Data for $FeTiO_3$ are after Wechsler & Prewitt (1984).

dered $R\bar{3}$ structures at ambient conditions is 0.78–0.76. Adoption of a $R\bar{3}$ structure by the $ZnTiO_3$ end member composition at ambient conditions has not been confirmed in our study, as this compound could not be synthesized.

Acknowledgements

This work is supported by the Natural Sciences and Engineering Research Council of Canada and Lakehead University (Canada). We thank Allan MacKenzie for assistance with analytical work, and Anne Hammond for sample preparation. We are grateful to Martin Kunz, an anonymous referee, and Robert F. Martin for their valuable comments on, and critical review of, the initial version of the manuscript.

References

Balić-Žunić, T. & Vicković, I. (1996): IVTON – a program for the calculation of geometrical aspects of crystal structures and some crystal chemical applications. *J. Appl. Crystallogr.* **29**; 305-306.

Barth, T.W. & Posnjak, E. (1934): The crystal structure of ilmenite. *Z. Kristallogr.* **A88**, 265-270.

Bartram, S.F. & Slepetys, R.A. (1961): Compound formation and crystal structure in the system ZnO–TiO_2. *J. Am. Ceram. Soc.* **44**, 493-499.

Birch, W.D., Burke, E.A.J., Wall, V.J. & Etheridge, M.A. (1988): Ecandrewsite, the zinc analogue of ilmenite, from Little Broken Hill, New South Wales, Australia, and the San Valentin mine, Sierra de Cartegena, Spain. *Mineral. Mag.* **52**, 237-240.

Dowty, E. (1999): Atoms 5.0. *Shape Software*, Kingsport, Tennessee 37663, USA; http://www.shapesoftware.com/

Gatehouse, B.M. & Nesbit, M.C. (1978): *Unpublished report.* Dept. Chem., Monash University, Clayton, Australia (not seen; secondary reference from Birch *et al.* (1988).

Goldschmidt, V.M. (1926): Geochemische Verteilungsgesetze der Elementer VII. *Skrifter Norsk Vidensk. Akad. Klas.* **1**. *Matematiks, Naturvidenskaplig Klasse*. Oslo, Norway.

JCPDS Powder Diffraction: Joint Committee for Powder Diffraction Standards (JCPDS). Swarthmore, Pennsylvania (now International Centre for Diffraction Data [ICDD], Newton Square, Pennsylvania), File Card No. 26–1500 ($ZnTiO_3$).

Kern, A.A. & Coelho, A.A. (1998): *Allied Publishers Ltd.* 144. http://www.bruker–axs.com TOPAS.

Kidoh, K., Tanaka, K., Marumo, F. & Takei, H. (1984): Electron density distribution in ilmenite-type crystals. II. Manganese (II) titanium (IV) trioxide. *Acta Crystallogr.* **B40**, 329-332.

Ko, Jaidong & Prewitt, C.T. (1988): High-pressure phase transformation in $MnTiO_3$ from the ilmenite to the $LiNbO_3$ structure. *Phys. Chem. Minerals* **15**, 355-362.

Linton, J.A., Fei, Yingwei & Navrotsky, A. (1999): The $MgTiO_3$–$FeTiO_3$ join at high pressure and temperature. *Am. Mineral.* **84**, 1595-1603.

Mitchell, R.H. (2002): *Perovskites: Modern and Ancient*. Almaz Press, Thunder Bay, Ontario (www.almazpress.com).

_____ & Liferovich, R.P. (2004): Zincian pyrophanite – ecandrewsite solid solution series and associated minerals from a lujavrite, Pilansberg alkaline complex, South Africa. *Can. Mineral.* **42**, 1169-1178.

Nakashima, K. & Imaoka, T. (1998): Niobian and zincian ilmenites in syenites from Cape Ashizuri, southwest Japan. *Mineral. Petrol.* **63**, 1-17.

Raymond, K.N. & Wenk, H.-R. (1971): Lunar ilmenite (refinement of the crystal structure). *Contrib. Mineral. Petrol.* **30**, 135-140.

Robinson, K., Gibbs, G.V. & Ribbe, P.H. (1971): Quadratic elongation: a quantitative measure of distortion in coordination polyhedra. *Science* **172**, 567–570.

Shannon, R.D. (1976): Revised effective ionic radii and systematic studies of interatomic distances in halides and chalcogenides. *Acta Crystallogr.* **A32**, 751-767.

Suwa, K., Enami, M., Hiraiwa, I. & Wang, Tai-Ming (1987): Zn–Mn ilmenite in the Kuiqi granite from Fuzou, Fujian Province, East China. *Mineral. Petrol.* **36**, 111-120.

SYONO, Y., AKIMOTO, S.-I., ISHIKAWA, Y. & ENDOH, Y. (1969): A new high pressure phase of $MnTiO_3$ and its magnetic property. *J. Phys. Chem. Solids* **30**, 1665-1672.

WECHSLER, B.A. & PREWITT, C.T. (1984): Crystal structure of ilmenite ($FeTiO_3$) at high temperature and high pressure. *Am. Mineral.* **69**, 176-185.

WHITNEY, D.L., HIRSCHMANN, M. & MILLER, M.G. (1993): Zincian ilmenite – ecandrewsite from a pelitic schist, Death Valley, California, and the paragenesis of (Zn,Fe)TiO_3 solid solution in metamorphic rocks. *Can. Mineral.* **31**, 425-436.

Received March 20, 2004, revised manuscript accepted September 27, 2004.

APPENDIX 1. SELECTED BOND-LENGTHS AND FRAMEWORK ANGLES OF SYNTHETIC $(Mn_{1-x}Zn_x)TiO_3$ SOLID-SOLUTION ($0.1 \le x \le 0.8$) AT AMBIENT CONDITIONS

			$x = 0$*	$x = 0.1$	$x = 0.3$	$x = 0.5$	$x = 0.7$	$x = 0.8$	$FeTiO_3$
A–Ti	Å		3.034(1)	3.022	3.014	3.005	3.003	3.001	2.944
A–*A*	Å	***a***	3.063(1)	3.060	3.056	3.049	3.044	3.041	3.003
A–*A*	Å	***b***	3.999(1)	3.980	3.948	3.922	3.893	3.881	4.074
Ti–Ti	Å	***a***	3.017(1)	3.009	3.002	2.996	2.992	2.990	2.993
Ti–Ti	Å	***b***	4.216(1)	4.223	4.197	4.167	4.131	4.110	4.124
O–O	Å	***c***	2.711(1)	2.720	2.719	2.712	2.708	2.704	2.701
O–O	Å	***d***	3.309(1)	3.299	3.281	3.270	3.250	3.242	3.216
O–O	Å	***e***	3.150(1)	3.152	3.139	3.108	3.097	3.105	3.052
O–O	Å	***f***	3.058(1)	3.054	3.046	3.018	3.017	3.031	3.005
O–O	Å	***g***	2.914(1)	2.900	2.897	2.892	3.894	2.895	2.921
O–O	Å	***h***	2.575(1)	2.565	2.556	2.563	2.551	2.529	2.607
O–O	Å	***i***	2.919(1)	2.906	2.887	2.888	2.864	2.840	2.886
Ti–O–*A*	°	***k***	118.76	119.15	119.25	119.18	119.21	119.10	119.78
A–O–*A*	°	***l***	88.41	88.30	88.46	88.91	88.99	88.80	89.07
Ti–O–Ti	°	***m***	99.08	99.15	99.22	98.96	99.16	99.60	97.92
Ti–O–*A*	°	***n***	125.99	125.78	125.86	125.76	126.01	126.30	128.01
Ti–O–*A*	°	***o***	87.97	87.52	87.38	87.38	87.39	87.45	86.62
Ti–O–*A*	°	***p***	137.18	137.22	136.82	136.81	136.17	135.67	135.65
BVS_A			2.061						2.033
BVS_{Ti}			3.987						3.988
BVS_O			2.016						2.122

$A = {}^{[VI]}(Mn_{1-x}Zn_x)$. The metal–metal distances: ***a*** across the shared edge between adjacent metal sites; ***b*** across the vacant octahedral position along [001]. The oxygen–oxygen distances: ***c*** *A*–Ti shared face; ***d*** *A* site, face opposite the shared face; ***e*** *A* site, shared edge; ***f*** *A*site, unshared edge; ***g*** Ti site, face opposite the shared face; ***h*** Ti site, shared edge; ***i*** Ti site, unshared edge. Framework angles: ***k***, ***n***, and ***p*** at the shared vertex; ***l*** and ***m*** at the shared edge; ***o*** shared face. * Data after Kidoh *et al.* (1984). Data for $FeTiO_3$ are after Wechsler & Prewitt (1984). BVS: bond-valence summation, expressed in valence units.